A mechanochemical synthesis of submicron-sized Li_2S and a mesoporous Li_2S/C hybrid for high performance lithium/sulfur battery cathodes

Xiang Li,[a] Mingxia Gao*[a], Wubing Du,[a] Yuanhe Wu,[a] Yongfeng Liu,[a] Hongge Pan,*[a] Congxiao Shang,[b] Zhengxiao Guo[c]

[a] State Key Laboratory of Silicon Materials, Key Laboratory of Advanced Materials and Applications for Batteries of Zhejiang Province & School of Materials Science and Engineering, Zhejiang University, Hangzhou 310027, P.R. China

[b]School of Environmental Sciences, University of East Anglia, Norwich, NR4 7TJ, UK

[c] Department of Chemistry, University College London, London, WC1H 0AJ, UK

Abstract

Lithium sulfide, Li_2S, is a promising cathode material for lithium-sulfur batteries (LSBs), with a high theoretical capacity of 1166 mA h g^{-1}. However, it suffers from low cyclic stability, low-rate capability and high initial activation potential. In addition, commercially available Li_2S is of high cost and of large sizes, over ten microns, which further exacerbates its shortcomings as sulfur cathodes. Exploring new approaches to fabricate small-sized Li_2S of low cost and to achieve Li_2S cathodes

*Corresponding authors. Tel./Fax: +86 571 87952615. E-mail addresses: gaomx@zju.edu.cn (M.Gao); hgpan@zju.edu.cn (H. Pan)

of high electrochemical properties is highly desired. This work reports a novel mechanochemical method to synthesize Li_2S of high purity and submicron in size by ball-milling LiH with sulfur in Ar atmosphere at room temperature. By further milling the as-synthesized Li_2S with polyacrylonitrile (PAN) followed by carbonization at 1000 °C for PAN, a Li_2S/C hybrid with nano-sized Li_2S embedded in a mesoporous carbon matrix is achieved. The hybrid with Li_2S as high as 74 wt% shows a high initial reversible capacity of 1020 mA h g^{-1} at 0.1 C and retains a capacity of 570 mA h g^{-1} after 200 cycles as a cathode material for LSBs. A capacity of 610 mA h g^{-1} is obtained at 1 C. The synthesis method of Li_2S is facile, environmentally benign, and of high output and low cost. The present work opens a new route in scalable fabrication of submicron-sized Li_2S and in the development of high performance Li_2S-based cathodes.

Keywords: lithium-sulfur batteries, lithium sulfide, mechanochemical synthesis, porous structure, electrochemical properties

Introduction

Rechargeable batteries possess great potential in the field of new energy applications.[1-5] Lithium sulfur battery (LSB) is one of the promising batteries due to its high theoretical energy density (1675 mA h g^{-1}), environment friendliness and low cost. [2,6-8] However, elemental S-based electrodes suffer from multiple limitations, including the low electrical conductivity of sulfur, the dissolution of the lithiation intermediates of polysulfides (Li_2S_n, $4 \leq n \leq 8$) in electrolyte, the (slow ?

complex? …need a “modifying word” before “shuttling) “shuttling” (maybe I’m not fully clear about this “shuttling” issue; shuttle is between the polysulfides at the cathode and the lithium sulfides (Li_2S_2/Li_2S) at the anode during cycling, and the large volume expansion of sulfur during its lithiation to Li_2S (*ca*. 79 vol%), all of which result in poor cycling stability and low rate capability; [1,9,10] the low melting point of S (115 °C), which limits its operation temperature; the necessity of using metallic lithium as anode, which causes safety concerns when dendritic lithium forms and penetrates through the separator during cycling.

Considerable effort has been devoted to solve these problems, such as encapsulation of sulfur in electrical conductive porous carbonaceous materials,[2,11,12] confinement of sulfur in high electron conductive frameworks,[4,13,14] or incorporation of a conductive polar metal oxides@carbon double layer coating on the surface of sulfur particles,[15] etc., which not only increases the electrical conductivity but also considerably alleviates the dissolution of polysulfides in electrolyte. In addition, optimizing electrolyte composition, such as adding $LiNO_3$ [16,17] and P_2S_5 [18] as additives; constructing new structured membrane or separator,[9,19] are also approaches with varied levels of effectiveness.

Compared with sulfur cathode, Li_2S offers several significant advantages as a cathode material for LSBs: it possesses a relatively high theoretical capacity of 1166 mA h g^{-1}; it can be paired with lithium-free anodes such as silicon and tin, readily alleviating the safety issues,[20] which also results in high specific energy density;[21] the melting point of Li_2S is high (938 °C), which can be operated at high temperatures;[22]

Li_2S transfers to sulfur with a relatively low volume shrink, considerably alleviating the volume change problem; Li_2S allows batteries to be assembled in the "discharged" state, a safer and more cost-effective process.[23] Nevertheless, similar as sulfur, Li_2S also suffers from low electronic and ionic conductivities, and the reaction intermediate polysulfides still suffer from the dissolution and "shuttling" problems. In addition, an extra shortcoming for Li_2S cathode is its high initial activation potential, especially for micron-sized Li_2S,[24-27] which causes an initial capacity utilization penalty.

Many approaches applicable for the improvement of the electrochemical performance of elemental sulfur-based cathodes are also applicable for Li_2S cathodes. Widely used is the incorporation of Li_2S with conductive carbonaceous materials[10,28-30] to increase the conductivity of the electrodes, and also to sequester the direct contact of Li_2S with electrolyte, hence alleviating the dissolution of polysulfides. In addition, designation of new current collector[31] and modification of electrolyte composition[32] are also effective as in the S-based cathode systems.

Nevertheless, commercially available Li_2S is commonly large in size, over ten microns, which creates a high activation barrier and slow kinetic properties. Reducing the particle size of Li_2S to nano-scale is essential to achieve high electrochemical performance, including obtaining an extremely low initial activation barrier of Li_2S.[10,33-35] The cyclic stress is also low for nano-sized Li_2S, favoring the integrity of the electrode,[37,38] thus also improves the cyclic stability and rate capability. However, as the high melting point of Li_2S, it becomes hard to allow the infiltration of Li_2S into

porous carbons as does sulfur in the sulfur-based cathode materials, forming carbon wrapped Li_2S/C hybrids with small confined Li_2S particles. Therefore, the method and the carbon host to fabricate nano-Li_2S/C composites are far from well developed.

Mechanical milling of commercial micron-sized Li_2S with electrical conductive carbon, such as carbon black, is a simple method of reducing the particle size of Li_2S and simultaneously incorporate conductive carbon.[38-40] However, the simply ball milled Li_2S/C mixtures still show relatively low cyclic stability. Further carbon coating by pyrolysis of pyrrole,[38,40] or further assisted with PVP (ployvinylpyrrolidone)[40] is necessary to achieve enhanced electrochemical properties. However, the obtained Li_2S/C products still not achieve favorable electrochemical properties as the size is insufficiently small for both Li_2S particles and Li_2S/C hybrid. Solution-based method is more widely used in fabricating nano-sized Li_2S recently, which is commonly combined with carbonaceous hosts simultaneously also, such as graphene/reduced graphene oxide (rGO),[26,33,36,37] carbon black[30] or carbonized polymer,[41] where commercial Li_2S is dissolved in an anhydrous solvent. The mainly used solvent is ethanol,[21,22,26,30,42] in addition, tetrahydrofuran (THF) is also used.[33] The Li_2S dissolved solutions were dropped on those carbonaceous hosts[36,37] or mixed with those carbonaceous materials.[26,33,41] After the solution was evaporated, Li_2S is re-precipitated, forming nano-sized particles throughout the carbonaceous hosts. A CVD carbon coating may be further prepared to achieve a high electrochemical performance of the nano-Li_2S/C systems.[26,36,41] Another widely reported method of synthesizing nano-sized Li_2S is to chemically react sulfur with $Li(CH_2CH_3)_3BH$ in

THF,[10,22,29,34] combining with in-situ loading of graphene[34] or graphene oxide (GO)[22] in THF, or a further surface carbon coating by CVD[10,22] or pyrolysis of polymer,[29] highly conductive carbon confined nano-Li_2S/C cathode materials with improved electrochemical performance are obtained. Nevertheless, as the commercial fabrication processes of Li_2S are also complicated and commonly performed at high temperatures,[42] commercial Li_2S is expensive. In addition, the reactant of $Li(CH_2CH_3)_3BH$ used in the aforementioned investigations is a much higher cost agent than Li_2S. Moreover, either the solution-based method or the chemical reaction method aforementioned needs scrupulous multistep process to obtained the final nano-sized Li_2S/C composites. Therefore, exploring facile approaches to fabricate small size of Li_2S of low cost and to further achieve high electrochemical properties of Li_2S-based cathode materials is highly desired.

This work reports a facile and high-output and environmentally benign approach to synthesize submicron-sized Li_2S of high purity by a mechanochemical reaction at room temperature via ball-milling LiH and sulfur in Ar atmosphere. No more chemical solutions or agents are needed. Li_2S and H_2 are the only two products. As the price of the staring material of LiH is almost 30 times lower than that of the commercial Li_2S (referred by Thermo Fisher Scientific Chemicals Co., Ltd), the synthetic method is hopefully economical. Meanwhile, the only by-product is highly pure H_2, which is of high value. Based on the as-synthesized Li_2S, Li_2S/C hybrids consisting of nano-sized Li_2S particles embedded in mesoporous carbon matrix are further synthesized by ball milling Li_2S with different contents of polyacrylonitrile

(PAN) followed by a carbonization of PAN. Given that PAN has a low melting temperature of 317 °C and it does not react with Li_2S at high temperature, this gives the way to coat Li_2S particles with molten PAN and hence with pyrolytic carbon after carbonization. As a result, the Li_2S/C hybrid with Li_2S as high as 74 wt% shows favorable electrochemical properties as cathode material for LSBs. The present work hopefully opens new routes in facile and scalable fabrications of small size Li_2S and high-performanced Li_2S/C cathode materials.

Experimental section

Syntheses of Li2S and Li_2S@C hybrids

Li_2S was synthesized via a mechanochemical reaction of LiH and S by ball-milling LiH (99%, Alfa aesar) with sublimated sulfur in a molar ratio of 2:1 for 24 h in vacuum with a rotating speed of 500 rpm. WC balls were used and the ball-to-sample ratio was 200:1. The synthesized Li_2S was further ball-milled with PAN in weight ratios of Li_2S: PAN = 3:1, 2:1 and 1:1 for 4 h in vacuum with a rotating speed of 500 rpm, forming mixtures, which are denoted as $3Li_2S$/PAN, $2Li_2S$/PAN and Li_2S/PAN, respectively. The mixtures were then heated to 1000 °C and maintained for 8 h in a flowing Ar atmosphere (2 L min^{-1}) at a heating rate of 2 °C min^{-1} to carbonize PAN, forming Li_2S/C hybrids. The fabrication process of the Li_2S/C composite is illustrated in scheme 1.

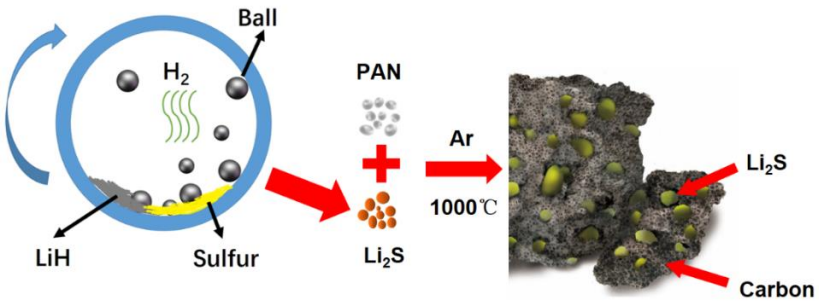

Scheme 1 Schematic illustration of the fabrications for Li_2S and Li_2S/C hybrid.

Material characterizations

Crystal structure of the samples was identified by X–ray diffraction (XRD, X'Pert PRO, PANalytical) using Cu-Ka radiation (λ=1.5418 Å) with a scanning step of 0.04º s^{-1}. Mass spectrum (MS) measurement of the gas in the milling jar after the milling of LiH and S was performed by a Hiden Analytical QIC-20 analyzer using pure Ar as a carrier gas. Morphologies of the samples were observed by scanning electron microscopy (SEM, Hitachi S-4800). The distribution of sulfur in the Li_2S/C hybrids was detected by energy-dispersive spectroscopy (EDS, Horiba) under SEM. The microstructure of the hybrids was further analyzed by high-resolution transmission electron microscopy (HRTEM, PhilipsFEI Tecnai G2 F30). Pore structure of the samples was analyzed by a nitrogen sorption method at 77 K on a Quantachrome Nova 1000e analyzer. Specific surface area of the samples was measured by the Brunauer-Emmet-Teller (BET) method using an adsorption branch in a relative pressure P/P_0 range from 0.00 to 1.0. The pore size distribution of the samples was calculated from the adsorption branch of the N_2 isotherm with the density functional theory (DFT). The carbon content of the samples was measured using an element

analyzer (EA GmbH, Vario Micro).

Electrochemical Tests

Electrochemical properties of the Li_2S/C hybrid were measured by using coin cells of CR2025 with Li foil (99.9%, Alfa Aesar) as the reference and counter electrode and a polyethylene membrane (Celgard 2400) as separator. The working electrode was prepared by pasting the mixed slurry of the Li_2S/C hybrid, Ketjen black, carbon black and polyvinylidene difluoride (PVDF, Alfa Asear) in a weight ratio of 75: 4: 11: 10 in 1-methyl-2-pyrrolidinone (NMP, Aldrich) on an aluminum foil using a blade coater, which was subsequently dried at 60 °C for 24 h in vacuum. The Li_2S loaded on each electrode was *ca*. 3 - 3.5 mg cm^{-2}. The electrolyte was a solution of 1 M bis (trifluoromethane) sulfonamide lithium salt (LiTFSI, Alfa Aesar) in mixed 1,3 dioxolane (DOL, Sigma-Aldrich) and dimethoxyethane (DME, Alfa Aesar) (v/v = 1:1) with 2 wt% lithium nitrate ($LiNO_3$, Alfa Aesar) as an additive. The cells were assembled in an argon-filled glove box with H_2O and O_2 contents less than 0.1 ppm (M-Braun, Germany).

The activation property of the Li_2S/C hybrids was tested by charging the cells from open-circuit voltage to 4.0 V vs. Li^+/Li at a current density of 0.05 C (1 C = 1166 mA g^{-1}) using an electrochemical testing system (Neware Technology Co., China). For the cyclic stability testing, the cells were galvanostatically discharged and charged in a potential rang of 3.0 - 1.0 V vs. Li^+/Li at 0.1 C after the initial activation at 0.05C. The rate capability of the Li2S/C hybrids was measured from 0.1 C to 5 C in the same potential range. The specific capacity of the cathodes was calculated on the

basis of Li_2S mass. Cyclic voltammetry measurements were carried out on coin cells at a scan rate of 0.1 mV s^{-1} in a potential rang from open-circuit voltage to 4.0 V in the first cycle and 3.0 - 1.0 V in the rest cycles (MSTAT-1, Arbin). Electrochemical impedance spectra (EIS) of the Li_2S/C electrodes were measured on the cells initially cycled for 4 cycles at 0.1 C at the state of charge in a frequency range from 10^{-1} to 10^6 Hz and a potentiostatic signal amplitude of 5 mV by using a frequency response analyzer (1255 B solarton) equipped with an electrochemical interface (1287, Solartron). All the electrochemical tests were performed at 25 ± 1°C.

Results and discussion

Structural characterization

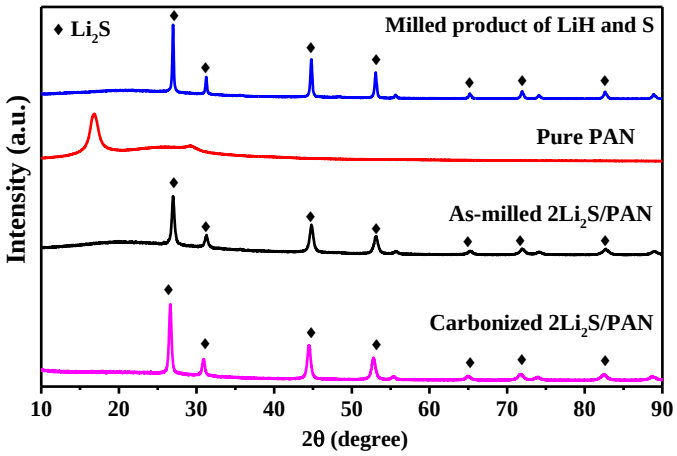

Fig. 1 XRD patterns of the milled products of LiH and S, the as-milled $2Li_2S$/ PAN mixture, the carbonized $2Li_2S$/PAN hybrid and the raw PAN.

The XRD pattern of the milled product of LiH and S is shown in Fig. 1. It is seen that Li_2S is the only detected phase, which demonstrates a full mechanochemical reaction of LiH and S, forming highly pure Li_2S. Mass spectrum of the gas in the milling jar (Fig. S1, supporting information) shows that there is only H_2 detected. The

reaction during milling is proposed as:

$$2LiH + S \xrightarrow{\text{Ball-miling}} 2Li_2S + H_2 \uparrow \quad (1)$$

The SEM image of the as-synthesized Li_2S is shown in Fig. S2. The particle size is less than 1 μm. It is proposed that the present method is facile, effective and scalable in producing highly pure submicron-sized Li_2S.

XRD analysis of the as-milled Li_2S-PAN mixtures with different weight ratios shows that Li_2S is the only detected phase in the milled mixtures, however, the peak width becomes broad compared with that of the as-synthesized Li_2S, indicating a lowered crystallinity of Li_2S after the milling. The patterns of the mixtures are similar. The representative one, which is from the $2Li_2S$/PAN mixture, is shown in Fig. 1. For comparison, the XRD pattern of raw PAN is also shown. It is found that the broad peak at 2θ of *ca*. 17° in the pattern of the raw PAN does not appear in the as-milled mixtures. The original structure of PAN was mostly destroyed during milling. Further XRD analysis of the carbonized products shows that there is also only Li_2S detected. However, the diffraction peaks of Li_2S become sharp, indicating an enhanced crystallinity of Li_2S during the carbonization process. The representative pattern of the carbonized products, which is from the $2Li_2S$/PAN system, is also shown in Fig. 1. It is noted that the carbonization temperature of 1000 °C is higher than the melting point of Li_2S (938 °C), therefore, Li_2S melts and re-solidified in the carbonization process. This is likely the main reason for the increasing crystallinity of Li_2S after the carbonization. Further by elemental analysis, the carbon contents of the products derived from the $3Li_2S$/PAN, $2Li_2S$/PAN and Li_2S/PAN mixtures are 19 wt%, 26 wt%

and 41 wt%, respectively, the products of which are denoted as Li_2S/19wt%C, Li_2S/26wt%C and Li_2S/41wt%C hybrids. Due to the amorphous feature of the PAN derived carbon, it cannot be detected by XRD.

Fig. 2a - c shows the SEM morphologies of the Li_2S/C hybrids. The images are directly from the as-carbonized products without any treatment, such as milling. It is seen that all the Li_2S/C hybrids show irregular particle shape, which are somewhat agglomerated. Among them, the Li_2S/26wt%C hybrid, derived from the $2Li_2S$/PAN mixture, shows the smallest particle size, most of which is smaller than 1 μm. Either higher content of PAN or lower content of PAN results in comparatively severer agglomeration up to several micrometers. Comparing with their original mixtures (Fig. S3), the $2Li_2S$/PAN mixture shows originally the smallest size. The Li_2S/C hybrids almost preserve the original particle distribution of the mixtures. In addition, for the Li_2S/19wt%C hybrid, there are two distinguishable morphologies as shown in Fig.2(a), a smooth one and a rough one, as marked by "1" and "2" in Fig. 2a, respectively. EDS analysis, as shown in the inset of the scanning map of sulfur, shows that the smooth particle is more S-richer than the rough one. It is obtained that the smooth particles are individual Li_2S and the rough particles are the combined Li_2S and carbon. However, individual Li_2S particles are hardly found in the other two hybrids with comparatively higher carbon contents. Li_2S particles are mostly embedded in the carbon matrix. Overall EDS analysis of the Li_2S/C hybrids under SEM shows that Li_2S particles are evenly distributed in the carbon matrixes (Fig. S3).

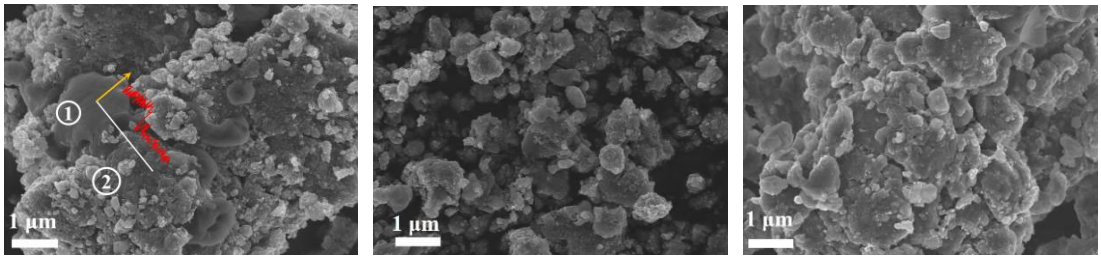

Fig. 2 SEM images of the Li_2S/C hybrids derived from: (a) 3Li_2S/PAN (19 wt%C); (b) 2Li_2S/PAN (26wt%C); (c) Li_2S/PAN (41 wt%C).

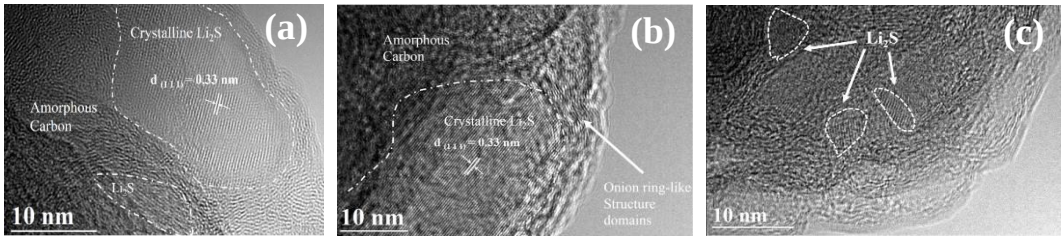

Fig. 3 HRTEM images of the Li_2S/26wt% C (a) and Li_2S/41 wt%C (b,c) hybrids.

Further HRTEM analysis shows that the Li_2S particles in the Li_2S/C hybrids are in sizes of several to several tens nanometers, much smaller than the original ones (Fig. S2), as shown in Fig. 3a–c, which are from the Li_2S/26wt%C and Li_2S/41wt%C hybrids. Crystal domains with lattice fringe of 0.33 nm are in good agreement with the (111) interplanar distance of Li_2S. Li_2S particles are dispersively embedded in the carbon matrix. Moreover, onion ring-like structure domains are observed in the carbon matrix, indicating a partial graphitization of the PAN derived carbon. PAN is a kind of ladder polymers, which can be pyrolyzed into cross-link carbon basal planes, favoring the formation of atomic size layered structure of carbon and hence resulting in a high electrical conductivity. [44,45]

(b)

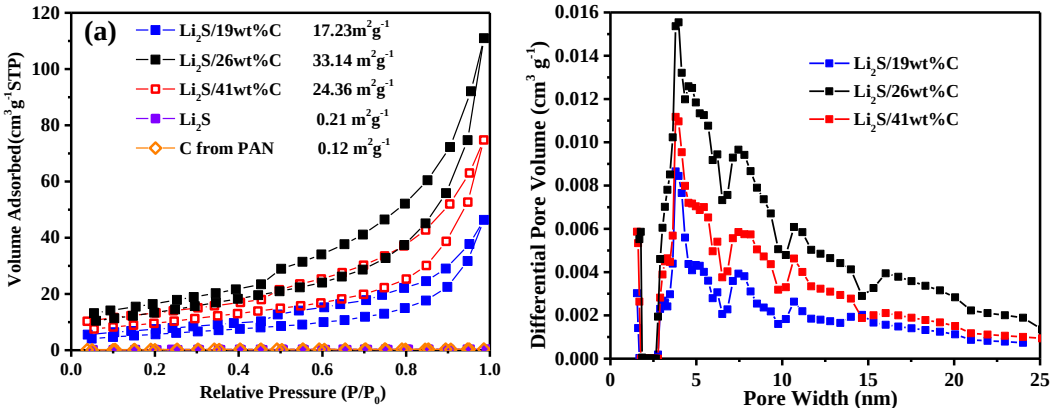

Fig. 4 (a) N_2 sorption isotherm curves of the Li_2S/C hybrids with different contents of carbon as well as the as-synthesized Li_2S and the individual PAN derived carbon; (b) Pore size distribution curves of the Li_2S/C hybrids.

Fig. 4a shows the nitrogen sorption curves of the Li_2S/C hybrids with different carbon contents at 77 K. For comparison, those of the individual PAN derived carbon and the as-synthesized Li_2S are also shown. It is seen that the Li_2S/C hybrids all illustrate the Ⅳ-type isotherms with a hysteresis loop at the relatively high pressure, which is the feature for mesoporous structures. Surface areas of the Li_2S/C hybrids as well as the as-synthesized Li_2S and the single carbonized PAN are listed in Fig. 4a. It is seen that the surface area of the Li_2S/C hybrids first increases and then decreases with the increase of the carbon content, reaching a maximum value of 33.14 m^2 g^{-1} for the Li_2S/26wt%C hybrid. The Li_2S/19wt%C and Li_2S/41wt%C hybrids show much lower surface areas of 17.23 and 24.36 m^2 g^{-1}, respectively. Moreover, there is almost no N_2 absorption for as-synthesized Li_2S and the individual PAN derived carbon as shown in Fig. 3a also, corresponding to low surface areas of 0.21 and 0.12 m^2 g^{-1}, respectively. It is inferred that the combination of Li_2S and PAN induces the mesoporous structure of the hybrids during the carbonization. Fig. 4(b) shows the

pore-size distribution curves of the Li_2S/C hybrids. The pore size ranges in 2 to 20 nm and concentrates in the range of 3 - 10 nm, mainly in *ca*. 4 - 5 nm. Among them, the Li_2S/26wt%C hybrid has the largest pore volume of 0.11 cm^3 g^{-1}. The pore volumes of the Li_2S/19wt%C and Li_2S/41wt%C hybrids are only of 0.02 and 0.08 cm^3 g^{-1}, respectively, which are extremely low, indicating an almost dense structure. The variation tendency of the pore size distribution, the pore volume and the surface areas of the hybrids are in good agreement. It is reported that PAN starts to melt at 317 °C and its carbonization is completed at 900 °C.[44] The melting point of Li_2S is 913 °C. It is likely that PAN melts and covers Li_2S particles before Li_2S melts. The pyrolysis of PAN can be divided into two main steps. The first step is at 150 - 500 °C and the second step is at 500 - 700 °C.[44] The first step consists of a cyclisation of the nitrile groups (C-N) and a cross-linking of the chain molecules; the second step consists a condensation reactions of the heterocyclic rings. These gases are supposed to induce mesopores in the carbon matrix with the existence of Li_2S, especially the molten Li_2S, though the actual mechanism is not clear yet.

Electrochemical properties

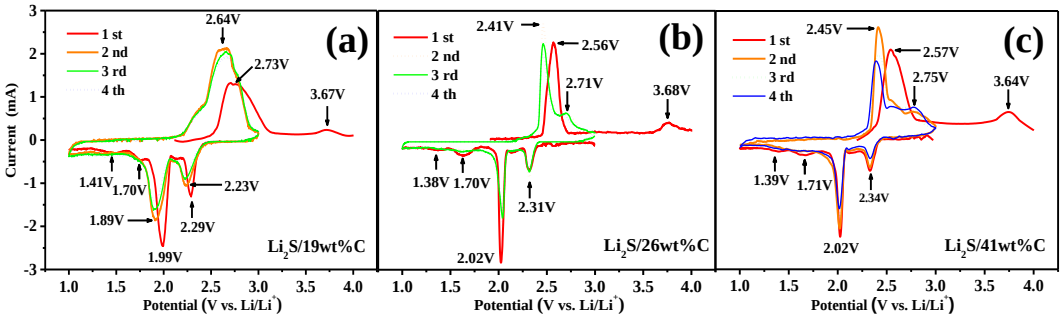

Fig. 5 CV profiles of the Li_2S/C hybrids with carbon contents of 19 wt%C (a), 26 wt% C (b) and 41 wt% C (c).

Fig. 5a - c shows the cyclic voltammograms of the Li_2S/C hybrids of the first 4 cycles at a scan rate of 0.1 mV s^{-1}. In the initial sweep, the hybrids all show one main anodic peak and two main cathodic peaks. In addition, there is one minor anodic peak and two minor cathodic peaks with extremely weak peak intensity. The main anodic peak is attributed to the oxidation of Li_2S to sulfur. The Li_2S/26wt%C and Li_2S/41wt%C hybrids show close anodic peak at 2.56 V and 2.57 V, respectively, but the former shows much shaper peak feature than the latter, indicating a better delithiation kinetics. While the Li_2S/19wt%C hybrid shows a higher anodic peak potential of 2.73 V, indicating a lower delithiation kinetics compared with the other two. The carbon content of 19 wt% is insufficient. The minor anodic peak at the high potential is found in other Li_2S/C systems also,[10,27,37] which is proposed from undesired parasitic reactions,[27] such as the delithiation of the largely agglomerated Li_2S particles.[10] In other studies, such weak anodic peak at the high potential is supposed due to the degradation of electrolyte[45] or the poor contact of Li_2S and carbon.[21] This peak is irreversible as it disappears in the following cycles as shown in Fig. 5, which is consistent with those reported in literature.[10,21,27,37] Anyway, the minor peak at the high potential is extremely weak. It is clear there is almost no evident initial energy/voltage barrier for the present hybrid.

The cathodic peaks centering at the comparatively low potential range of 2.29 - 2.34 V for the different hybrids in the first sweep correspond to the conversion of sulfur to polysulfides, where the potential tends to be at slightly higher value for higher carbon content. The cathodic peaks centering at the relatively lower potential

range of 1.99 - 2.02 V are attributed to the further reduction of the polysulfides to Li_2S_2 and/or further to Li_2S. The latter shows much high intensity than the former, indicating that more capacities are generated from this reaction. The two main cathodic peaks show close peak potential for the three hybrids, indicating that the lithiation ability of sulfur to polysulfides and then to Li_2S_2/Li_2S are not evidently different for the hybrids in the first sweep. As it is proposed that there was irreversible reduction of $LiNO_3$ occurring at potentials lower than 1.7 V (vs. Li/Li^+),[46] the two minor cathodic peaks in the initial sweep here is likely also due to the irreversible reduction of $LiNO_3$. In addition, the main cathodic peak potentials of the Li_2S/26wt%C and Li_2S/41wt%C hybrids are almost stable upon cycling, indicating a lower lithiation polarization. Whereas the Li_2S/19wt%C hybrid shows decreased peak potential from the first sweep to the second one, indicating an increasing lithiation polarization. Moreover, the main anodic peaks of all the hybrids move to lower potentials due to the activation during the first charge process, where the Li_2S/26wt%C hybrid reaches the lowest value of 2.41 V, and the Li_2S/19wt%C and Li_2S/41wt%C hybrids shift to 2.64 and 2.45 V, respectively. However, the potential difference between the first and the second sweep of less than 0.15 V is almost negligible compared with the commercial Li_2S cathode,[21] and are also much smaller than other nano-Li_2S/C cathode systems[39,47] and the P_2S_5-activiated Li_2S system.[24] After the second sweep, both anodic and cathodic peak positions of all the hybrids keep almost stable, demonstrating a stable and small redox polarization. Cell polarization is supposed mainly due to the dissolution of polysulfides into the

electrolyte and the deposition of Li_2S on the electrode in Li/S batteries.[48] The low redox polarization of the present hybrids is mainly attributed to the almost fully wrapping of nano-Li_2S particles by carbon, which alleviates the dissolution of polysulfides into the electrolyte and thence the less deposition of Li_2S on the electrode. In addition, there is a new weak anodic shoulder peak centering at 2.71 V and 2.73 V from the second cycle for the hybrids with carbon contents of 26 wt% and 41 wt%, respectively, which is proposed due to the conversion of polysulfides to element sulfur in the case that the product of the prominent oxidation of Li_2S is high-order polysulfides.[42,49] The further oxidation is supposed due to the high electron conductivity and low polarization. One single anodic peak is also found in other Li_2S/C system,[40] which is attributed to the oxidation of Li_2S to long-chain polysulfides. For the Li_2S/19wt%C hybrid, there is a shoulder peak at the comparatively lower potential partially overlapped with the dominated anodic peak at the comparatively higher potential after the initial sweep, but without the weak shoulder peak at the right side of the dominated anodic peak as in the other two hybrids. This is probably attributed to a two-step oxidation of Li_2S to different orders of polysulfides, and the further oxidation of polysulfides to sulfur is restrained. As an overall, the anodic peaks of the Li_2S/19wt%C hybrid for the different cycles are all much broader and the peak position located at much higher potentials than those of the other two, indicating a much lower oxidation kinetics and a higher polarization, which is due to it less high electronic conductivity as there are Li_2S particles exposing out the carbon matrix, without the intimate contact to the carbon matrix, and the large

particle size of the hybrid as shown in Fig. 2a.

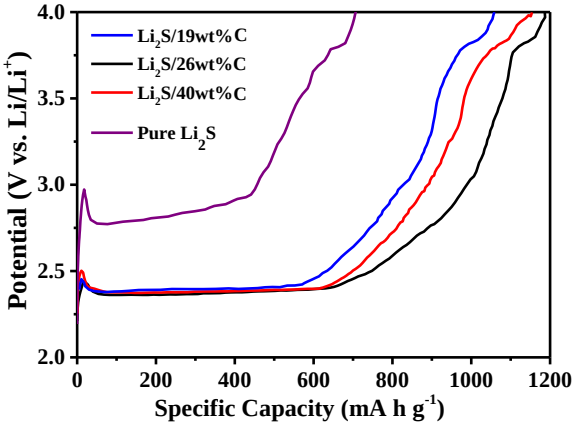

Fig. 6 Charge profiles of the activation process of the Li_2S/C hybrids as well as the as-synthesized Li_2S.

The charge profiles of the activation process of the Li_2S/C hybrids as well as the as-synthesized Li_2S are shown in Fig. 6, where the cells were charged from open-circuit voltage to 4 V at a current density of 0.05 C. It is seen that all the Li_2S/C hybrids show an overpotential at ca. 2.45 V and a flat charge plateau at ca. 2.38 V, with a negligible potential barrier less than 0.1 V. Whereas the as-synthesized Li_2S shows an overpotential at ca. 2.98 V, followed by a gradually increased plateau from ca. 2.76 V, with a potential barrier of 0.22 V. The extremely small activation barrier of the Li_2S/C hybrid is attributed to the superfine nano-sized Li_2S particles which are well embedded in the carbon matrix and their intimate contact with the carbon matrix. The result is also in good agreement with that obtained from the CV analysis. Though the as-synthesized bare Li_2S has a higher overpotential and a higher charge plateau than the Li_2S/C hybrids, the value is still much lower than the ca. 3.5 V of the commercial micro-sized Li_2S,[21] solution synthesized pure nano-Li2S and Li_2S/graphene composite,[26] ball-milled commercial Li_2S[27] and ball-milled commercial

Li_2S with multi-wall carbon nano- tubes (MWCNTs).[50] The originally better activation ability and the delithiation ability of the as-synthesized Li_2S than those aforementioned Li_2S is likely due to its originally small particle size. Moreover, Li_2S is highly sensitive to moisture and oxygen, which is easily to form a stable LiOH surface layer coupled with an unstable S-H native layer during operation. The formation of LiOH on the surface of the Li_2S particles hinders the diffusion of lithium ions during electrochemical reaction. Annealing treatment at temperature higher than 650 °C, higher than the melting point of 462 °C of LiOH, is supposed to be able to remove the LiOH layer.[51] It is probably that the carbonization process of PAN at 1000 °C purifies the surface of Li_2S, and hence results in extra action in the reductions of the overpotential and the potential of the charge plateau of the Li_2S/C hybrids.

Moreover, the Li_2S/26wt%C hybrid shows the largest activation capacity of 1183 mA h g^{-1} among the three hybrids, slightly higher than the theoretical capacity of Li_2S, which is supposed due to some side reactions at the high potential range. The Li_2S/19wt%C hybrid shows the lowest activation capacity of 1026 mA h g^{-1}, which is also only slightly lower than the theoretical capacity of Li_2S. Whereas the bare Li_2S not only shows a high charge plateau but also a much lower activation capacity of 704 mA h g^{-1}. The result demonstrates that there is almost no activation barrier and it is facile to be activated for the porous carbon hosted Li_2S nano-particles, especially for the Li_2S/26wt%C hybrid. The relatively lower carbon content (19 wt%) results in lower electronic conductivity and the higher carbon content (41 wt%) results in a

large particle size of the hybrid and a thick carbon layer around the Li_2S particles, both of which should not facilitate the diffusion of lithium ion and is unfavorable to the activation of Li_2S.

The cycling performance and the Coulombic efficiency of the Li_2S/C hybrids at 0.1 C after an initial charge activation at 0.05 C up to 4.0 V are shown in Fig. 7a. The initial reversible capacities of the Li_2S/C hybrids are 919, 971 and 953 mA h g^{-1}, respectively, for the carbon contents of 19, 26 and 41 wt%, and the capacities retains

(a)

288, 570 and 457 mA h g^{-1} after 200 cycles, corresponding to capacity retentions of 31%, 56% and 48%. In addition, the initial Coulombic efficiencies of the hybrids are correspondingly 85%, 90% and 88%, which seem not high. However, the Coulombic efficiency of all the hybrids increases gradually in the initial several to several tens cycles and reaches a stable value of ca. 95 - 96%. Especially for the Li_2S/26wt%C hybrid, less cycles are needed for reaching a high stable value of 96%, as seen from Fig. 7a. The above electrochemical properties of the hybrids all first increase and then decrease with the increase of the carbon contents, where the Li_2S/26wt%C hybrid shows the highest capacity, capacity retention and the Coulombic efficiency.

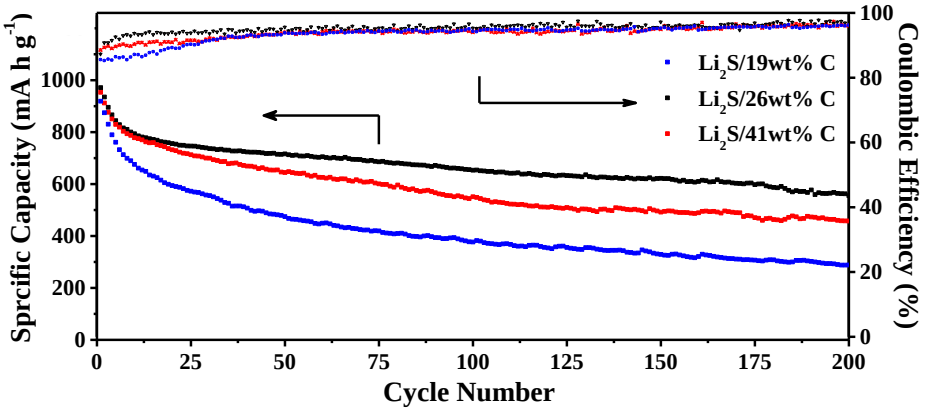

(b)

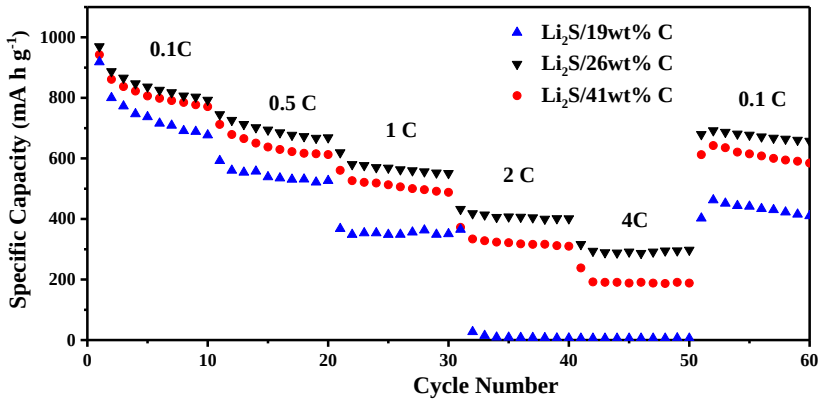

Fig. 7 Cyclic stability at 0.1 C (a) and rate capability (b) of the Li_2S/C hybrids with different carbon contents.

The rate capability of the Li_2S/C hybrids up to 4C are shown in Fig. 7b. The Li_2S/26wt%C hybrid shows the highest capacities at the different discharge rates, achieving capacities of 746, 610, 434 and 270 mA h g^{-1} at 0.5 C, 1C, 2Cand 4 C, respectively. A discharge capacity of 690 mA h g^{-1} is recovered when the current density is reduced back to 0.1 C, which is still high, though there is capacity fading after the cycling at the different rates. In comparison, the Li_2S/19wt%C hybrid fails to cycle at 2 C and the capacity is only 340 mA h g^{-1} at 1 C. The Li_2S/41wt%C hybrid shows capacities of 707, 530, 380 and 204 mA h g^{-1} at 0.5C, 1C, 2C and 4C, respectively, all lower than those of the Li_2S/26wt%C hybrid.

The exposure of the Li_2S particles out the carbon matrix and the large particle size of the hybrid, which results in low electronic conductivity and sever dissolution of the polysulfides to the electrolyte and low lithium ion diffusion, is supposed to be the main reason for the lowest electrochemical properties of the Li_2S/19wt%C hybrid. Whereas the highest electrochemical properties of the Li_2S/26wt%C hybrid are attributed to its unique structure, where nano Li_2S particles are well embedded in the

partially graphitic mesporous carbon matrix, which offers high electron conductivity and alleviates the dissolution of the polysulfides into the electrolyte, and also facilitates the lithium ion diffusion. With further increasing the carbon content to 41 wt%, the particle size of the Li_2S/C hybrids increases. Moreover, the carbon layers around the Li_2S particles become thick and the amounts of pores and the surface areas are reduced. All of those block the penetration of the electrolyte, resulting in less effective lithium ion diffusion and low utilization of the active material, thence, the reduced electrochemical properties.

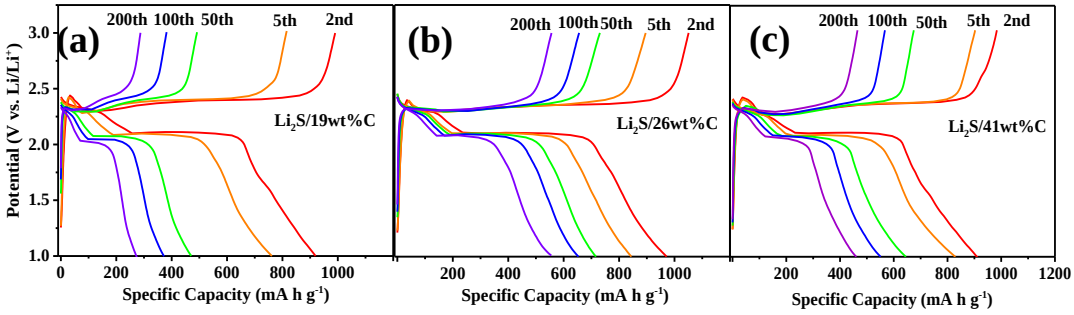

Fig. 8 Voltage profiles at 0.1 C of the Li_2S/C hybrids with different carbon contents of selected cycles after an initial activation: (a) 19wt%C; (b) 26wt%C; (c) 41wt%C.

Voltage profiles of the Li_2S/C hybrids of selected cycles up to 200 cycles at 0.1C after an initial activation at 0.05 C are shown in Fig. 8. The Li_2S/19wt%C hybrid shows two charge plateaus, a short flat plateau at 2.3 V followed by a comparatively long and slightly increasing plateau from ca. 2.3 V to 2.4 V, which is consistent with the CV curve that there is a split broad anodic peak after the initial sweep. Only one distinguishable charge plateau can be observed for the other two hybrids, which is at an almost same potential of 2.3 V, corresponding to the one prominent anodic peak at their CV curves. The weak shoulder peak at the right side of the main anodic peak is

not reflected at the charge plateau, due probably the less discrimination of the weak delithiation of the charge plateau compared with the CV profile. Furthermore, the charge plateau potentials of the Li_2S/26wt%C and Li_2S/41wt%C hybrids are all highly overlapped for the 200 cycles, indicating a low and stable delithiation polarization, whereas that of the Li_2S/19wt%C hybrid is gradually increased during cycling, indicating an increasing polarization. There are two discharge plateaus for all the hybrids. The sloping one at the comparatively high potential range corresponds to the lithiation of sulfur to lithium polysulfides, and the flat one at the comparatively low potential corresponds to the further reduction of the polysulfides to Li_2S_2 or Li_2S. The latter process is the first main one, which generates more capacity compared with the former. The subsequent sloping curve from the plateau potential to the bottom cut-off potential is the further reduction of Li_2S_2 to Li_2S. Moreover, the discharge plateaus of the Li_2S/26wt%C and Li_2S/41wt%C hybrids are almost stable upon cycling to 200 cycles, especially for the former, demonstrating an extremely limited increasing lithiation polarization during cycling. Whereas the discharge plateaus of the Li_2S/19wt%C hybrid shift to slightly lower potentials upon cycling, indicating an increasing lithiation polarization.

Further electrochemical impedance spectroscopy (EIS) analysis, Fig. 9, shows that the charge-transfer resistance of the electrode surface (R_{ct}) of the Li_2S/26wt%C hybrid is only 45 Ω, whereas those of the Li_2S/19wt%C and Li_2S/41wt%C hybrid are of much higher of 141 and 75 Ω, respectively, as obtained from the Z-fitted equivalent circuit as the inset in Fig. 9, where R_s represents the solution resistance of the

electrolyte and CPE is related to the solid-state diffusion of Li^+ in the double layer capacitor between the electrolyte and the cathode interface. *W* is the Warburg impedance related to the diffusion of lithium ions in the active materials. The lowest R_{ct} value of the Li_2S/26wt%C hybrid indicates the highest electronic conductivity and reaction kinetics, which is consistent with its highest rate capability. The result further demonstrates that the Li_2S/26wt%C hybrid has favorable electronic contact between the embedded Li_2S particles and the carbon matrix. The relatively highly porous thin carbon layer wrapped around the Li_2S particles facilitates the lithium ion diffusion.

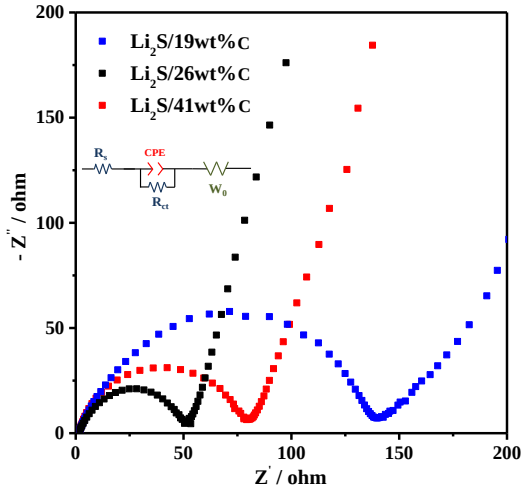

Fig. 9 Nyquist plots of the Li_2S/C hybrids with different carbon contents.

The comparison of the capacity and capacity retention of the present Li_2S/26wt%C hybrid (derived from the $2Li_2S$/PAN mixture) with some recently reported representative Li_2S/C systems is shown in Table 1. Comparing the capacity of the Li_2S/C systems at the 0.1C after the comparable cycle numbers, the present one shows higher retained capacity than the nano-Li_2S/C systems prepared by chemical reaction in THF,[29]solution based re-precipitated 3D-rGO-Li2S system further carbon coated by the pyrolysis of PVP.[53] Though the present retained capacity after the

comparable cycles is inferior to the those Li_2S/C systems, [28, 34, 37, 40] however, the Li_2S content and the Li_2S loading on the electrode of the present system is much higher than those systems, which commonly results in lower apparent specific capacity and cyclic stability. Moreover, it is no doubt that low Li_2S content of the Li_2S/C system will reduces the volumetric specific capacity, which is undesired for practical application. As different charge and discharge rates are used in some other studies,[30,36,52] the capacities and capacity retention cannot be usefully compared. However, the high rate capability of the present Li_2S/26wt%C hybrid is superior to the electrospinning fabricated nano-Li_2S/CNFs[52] and solution re-precipitation prepared Li_2S/C further carbon coated by CVD,[30] but is inferior to the solution reaction prepared Li_2S/GO[22] and solution re-precipitation prepared Li_2S/graphene[36] further carbon coated by CVD. However, as the Li_2S contents and the Li_2S loading on the electrode are also much lower for the two system[22,36] compared with those of the present system, it is supposed that there should not be so large rate capability different between the present system and the reported systems as from the apparent data. Considering the present fabrication method for the Li_2S/C hybrid is facile and low cost, it is hopeful helpful in the further development of Li_2S/C cathode materials for high performance LSBs.

Table 1 Comparison of the electrochemical properties of the present Li_2S/26wt%C hybrid and some reported Li_2S/C cathodes.

Systems	Carbon resource	Current rate(C)	Li_2S contents	Li_2S loading	1st reversible	Cycle number	Capacity after the	Refs.

			(wt%)	(mg cm^{-2})	capacity (mA h g^{-1})		reported cycles (mA h g^{-1})	
Li_2S/C	pyrolytic PAN	0.1	74	3-3.5	1020	200	570	Our work
Li_2S/C	pyrolytic PAN	0.1	74	3-3.5	1020	100	638	Our work
Li_2S/GO@C	GO/CVD carbon coating	0.2	60	0.7-0.9	964	50	700	22
Li_2S/CNT	CNT	0.1	37	2	838	100	680	28
Li_2S/C	pyrolytic [Emim]-[$N(CN)_2$]	0.1	NA	2.5-3	826	50	680	29
Li_2S@C	Carbon black/CVD carbon coating	0.2	72	~2.8	758	200	536	30
Li_2S/Graphene	Graphene	0.1	53	1.3	~920	100	791	34
Li_2S/Graphene@C	Graphene/CVD carbon coating	0.5	55	1-1.5	720	700	700	36
Li_2S/rGO	rGO paper	0.1	50-60	0.8-1.6	1119	150	816	37
Li_2S/CB@NC	Carbon black/ pyrolytic PVP carbon coating	0.1	70	0.8	1020	200	660	40
Li_2S/CNF	CNF	0.025/0.5	72	1.5	800/630*	100	510	52
3D-rGO-Li_2S@C	rGO/ pyrolytic PVP carbon coating	0.1	75	2.5-3.5	856	100	560/65	53

Note: * the initial capacity is tested at 0.025 C is 800 mA h g^{-1}, and the first capacity at 0.5 is ca. 630 mA h g^{-1}.

Conclusions

An effective mechanochemical method of synthesizing submicron-sized Li_2S of high purity is developed by simply ball-milling of LiH with sulfur in Ar atmosphere at room temperature. The as-synthesized Li_2S is further applied as a cathode material for LSBs in combination with polyacrylonitrile (PAN) via ball milling followed by a carbonization at 1000 °C for PAN. Carbon contents of 19 - 41 wt% for the Li_2S/C hybrids with nano-sized Li_2S particles embedded in mesoporous carbon matrixes are obtained by adjusting the staring weight ratios of Li_2S and PAN. As cathode material

for LSBs, the hybrids all shows extremely low activation overpotential. The one with Li_2S as high as 74 wt% shows a high initial reversible capacity of 1020 mA h g^{-1} at 0.1 C and retains a capacity of 570 mA h g^{-1} after 200 cycles. A capacity of 610 mA h g^{-1} is obtained at 1 C. Both fabrication methods of Li_2S and nano-sized Li_2S/C hybrids are facile, high-output, environmentally benign and low-cost. The favorable electrochemical properties of the Li_2S/26wt%C hybrid are attributed to its unique structure, where the nano-sized Li_2S particles are well wrapped by carbon shell which effectively alleviates the dissolution of polysulfides to the electrolyte, and the partially graphitic mesoporous carbon facilitates the migration of both electrons and lithium ions, favoring the delithiation/lithiation and enhancing the utilization of Li_2S. Whereas either higher or lower carbon contents of 19 wt% or 41 wt% all reduced the electrochemical properties due to the larger particle size of the hybrids and the insufficient electronic conductivity for the former and the low lithium ion diffusion ability for the latter. The present work is hopefully helpful in developing facile route in fabrication of small size Li_2S and in the development of high performance Li_2S-based cathodes.

Acknowledgments

The work was supported by the National Natural Science Foundation of PR China (Nos. 51571178, 51571175 and 51371158), National Materials Genome Project (No. 2016YFB0700600), Pao Yu-Kong International Fund, Zhejiang University and the UK EPSRC (Nos. EP/K002252/1 and EP/K021192/1).

References

1 Y. Yang, G. Zheng and Y. Cui, *Chem. Soc. Rev.*, 2013, **42**, 3018.

2 Z. Li, H. W. Bin and X. W. Lou, *Energy Environ. Sci*., 2016, **9**, 3061.

3 M. X. Gao, D. S. Wang, X. Q. Zhang, H. G. Pan, Y. F. Liu, C. Liang, C. X. Shang and Z. X. Guo, *J. Mater. Chem. A*, 2015, **3**, 10767.

4 Z. Li, J. T. Zhang, Y. M. Chen, J. Li and X. W. Lou, *Nat. Commun.*, 2015, **6**, 8850.

5 S. M. Zhang, H. T. Gu, H. G. Pan, S. H. Yang, W. B. Du, X. Li, M.X. Gao, Y. F. Liu, M. Zhu, L. Z. Ouyang, D. C. Jian and F. Pan, *Adv. Energy Mater*., 2016, 1601066.

6 A. Manthiram, S. H. Chung and C. X. Zu, *Adv. Mater*., 2015, **27**, 1980.

7 M. F. Chen, X. Y. Wang, S. Y. Cai, Z. Y. Ma, P. Song and A. C. Fisher, *J. Mater. Chem. A*, 2016, **4**, 16148.

8 Q. Zhao, X. F. Hu, K. Z. Zhang, N. Zhang, Y. X. Hu and J. Chen, *Nano lett.*, 2015, **15**, 721.

9 L. Luo, S. H. Chung and A. Manthiram, *J. Mater. Chem. A*, 2016, **4**, 16805.

10 C. Y. Nan, Z. Lin, H. G. Liao, M. K. Song, Y. D. Li and E. J. Cdairns, *J. Am. Chem. Soc.*, 2014, **136**, 4659.

11 N. Jayaprakash, J. Shen, S. S. Moganty, A. Corona and L. A. Archer, *Anges. Chem. Int. Ed.*, 2011, **50**, 5904

12 Y. H. Wu, M. X. Gao, X. Li, Y. F. Liu and H. G. Pan, *J. Alloys Compd.*, 2014, **608**, 220.

13 J. K. Wang, K. Q. Yue, X. D. Zhu, K. L. Wang and L. F. Duan, *Phys. Chem. Chem. Phys.*, 2016, **18**, 261.

14 F. Gao, J. Y. Qu, Z. B. Zhao and J. S. Qiu, *J. Mater. Chem. A*, 2016, **4**,16219.

15 Z. Li, J. T. Zhang, B. Y. Guan, D. Wang, L. M. Liu and X. W. Lou, *Nat. Commun.*, 2016, **7**, 13065.

16 Y. V. Mikhaylik, U.S. Patent, 2008, 7352680.

17 D. Aurbach, E. Pollak, R. Elazari, G. Salitra, C. S. Kelley, and J. Affinito, *J. Electrochem. Soc.*, 2009,156, A694.

18 Z. Lin, Z. C. Liu, W. J. Fu, N. J. Dudney and C. D. Liang, *Adv. Funct. Mater.*, 2013, **23**, 1064.

19 X. X. Gu, C. Lai, F. Liu, W. L. Yang, Yang Long Hou and S. Q. Zhang, *J. Mater. Chem. A*, 2015, **3**, 9502.

20 Z. Lin, Z. C. Liu, W. J. Fu, N. J. Dudney and C. D. Liang, *ACS. Nano*, 2013, **7**, 2829.

21 Y. Yang, G. Y. Zheng, S. Misra, J. Nelson, M. F. Toney, Y. Cui, *J. Am. Chem. Soc.*, 2012, **134,** 15387.

22 Y. Hwa, J. Zhao and E. J. Cairns, *Nano Lett.*, 2015, **15**, 3479.

23 Y. X. Yin, S. Xin, Y. G. Guo and L. J. Wan, *Angew. Chem., Int. Ed.*, 2013, **52**, 13186.

24 C. X. Zu, M. Klein and A. Manthiram, *J. Phys. Chem. Lett.*, 2014, **5**, 3986.

25 Z. W. She, J. H. Yu, W. Y. Li, P. C. Hsu, H. T. Wand, Y. M. Sun, H. B. Yao, Q. F. Zhang and Y. Cui, *Nat. Commun.*, 2014, **5**,5017.

26 F. X. Wu, J. T. Lee, A. Magasinski, H. Kim and G. Yushin, *Part. Part. Syst. Charact.*, 2014, **31**, 639.

27 J. Liu, H. Nara, T. Yokoshima, T. Momma, T. Osaka, *J. Power Sources.*, 2015, **273**, 1136.

28 Y. Z. Fu, Y. S. Su and A. Manthiram, *Adv. Energy Mater*., 2014, **4**, 1300655.

29 L. Suo, Y. J. Zhu, F. D. Han, T. Gao, C. Luo, X. L. Fan, Y. S. Hu and C. S. Wang, *Nano Energy.*, 2015, **13**, 467.

30 T. Yang, X. L. Wang, D. H. Wang, S. H. Li, D. Xie, X. Q. Zhang, X. H. Xia and J. P. Tu. *J. Mater. Chem. A,* 2016, **4**, 16653.

31 S. Zhang, M. Liu, F. Ma, F. M. Ye, H. F. Li, X. Y. Zhang and Y. G. Zhang, *J. Mater. Chem. A*, 2015, **3**, 18913.

32 R. Xu, X. F. Zhang, C. Yu, Y. Rem, J. C. M. Li and I. Belharouak, *ChemSusChem*., 2014, **7**, 2457.

33 K. Han, J. M. Shen, C. M. Hayner, H. Q. Ye, M. C. Kung and H. H. Kung, *J. Power Sources*, 2014, **251**, 331.

34 K. Zhang, L. J. Wang, Z. Hu, F. Y. Cheng and J. Chen, *Sci. Rep.*, 2014, **4**, 6467.

35 S. K. Lee, Y. J. Lee and Y. K. Sun, *J. Power Sources*, 2016, **323**, 174.

36 F. X. Wu, J. T. Lee, E. Zhao, B. Zhang and G. Yushin, *ACS Nano*, 2016, **10**, 1333.

37 C. Wang, X. S. Wang, Y. Yang, A. Kushima, J. Chen, Y. H. Huang and J. Li, *Nano Lett*., 2015, **15**, 1796.

38 L. Chen, Y. Z. Liu, M. Ashuri, C. H. Liu and L. L. Shaw, *J. Mater. Chem. A*, 2014, **2**, 18026.

39 K. P. Cai, M. K. Song, E. J. Cairns and Y. G. Zhang, *Nano Lett*., 2012, **12**, 6474.

40 L. Chen, Y. Z. Liu, F. Zhang, C. H. Liu and L. L. Shaw, *ACS Appl. Mater.*

Interfaces, 2015, **7**, 25748.

41 J. J. Chen, Q. Zhang, Y. N. Shi, L. L. Qin, Y. Cao, M. S. Zhen and Q. F. Dong, *Phys. Chem. Chem. Phys.*, 2012, **14**, 5376.

42 X. M. Li, C. A. Wolden, C. M. Ban and Y. G. Yang, *ACS Appl. Mater. Interfaces*, 2015, **7**, 28444.

43 M. Jing, C. G. Wang, Q. Wang, T. J. Bai and B. Zhu, *Polym. Degrad. Stab*., 2007, **92**, 1737.

44 N. Yusof, A. F. Ismail, *J. Anal. Appl. Pyrolysis*, 2012, **93**,1

45 S. Meini, R. Elazari, A. Rosenman, A. Garsuch and D. Aurbach, *J. Phys. Chem. Lett*., 2014, **5**, 915.

46 S. S. Zhang, *J. Electrochem. Soc*., 2012, **159**, A920.

47 S. Liang, C. Liang, Y. Xia, H. H. Xu and Y. P. Gan, *J. Power Sources*, 2016, **306**, 200.

48 H. Lu, K. Zhang, Y. Yuan, F. R. Qin and Y. Q. Lai, *Electrochim. Acta.*, 2015, **161**, 55

49 Z. Li, L. X. Yuan, Z. Q. Yi, Y. Liu and Y. H. Huang, *Nanoscale*, 2014, **6**, 1653.

50 M. R. Kaiser, X. Liang, H. K. Liu, S. X. Dou, J. Z. Wang, *Carbon*, 2016, **103**, 163.

51 Y. S, J. S. Lee, Y. Son, J. H. Jang and J. Cho, *Adv. Energy Mater*., 2015, **5**, 1500110.

52 F. M. Ye, Y. Hou, M. N. Liu, L. S. Zhou, H. F. Li and Y. G. Zhang, *Nanoscale*, 2015, **7**, 9472

53 D.H. Wang, D. Xie, T. Yang, Y. Zhong, X.L. Wang, X.H. Xia, C.D. Gu, J.P. Tu，*J.*

Power Sources., 2016, **313**, 233.